J. Mol. Biol. (1994) **240**, 127–137

Structure Determination of an Fab Fragment that Neutralizes Human Rhinovirus 14 and Analysis of the Fab-Virus Complex

Hansong Liu[1], Thomas J. Smith[1]†, Wai-ming Lee[2], Anne G. Mosser[2], Roland R. Rueckert[2], Norman H. Olson[1], R. Holland Cheng[1] and Timothy S. Baker[1]

[1]*Department of Biological Sciences, Purdue University West Lafayette, IN 47907-1392, U.S.A.*

[2]*Institute for Molecular Virology, University of Wisconsin 1525 Linden Drive, Madison, WI 53706, U.S.A.*

The crystal structure of Fab17-IA, an antigen-binding fragment from a murine immunoglobulin that neutralizes human rhinovirus 14 (HRV14), has been solved to 2·7 Å resolution. Fab17-IA crystallized into three different space groups depending upon the method used to purify the intact antibody. The structure was determined by use of molecular and isomorphous replacement methods. The current model has a crystallographic *R*-factor of ~19% for 10,192 independent reflections between 8 and 2·7 Å. Correlation coefficient calculations showed that the Fab17-IA structure can be fit into the Fab17-IA/HRV14 image reconstruction density to within 5 Å positional accuracy and to within a few degrees of rotation. The resulting interface of the docked antibody was examined and showed extensive charge and shape complementarity with the virus surface that was supported by site-directed mutagenesis experiments. The success of this approach validates the utility of combining X-ray crystallography with cryo-electron microscopy of complex macromolecular assemblies.

Keywords: human rhinovirus; immunoglobulin; neutralization; crystallography; Fab–virus complex

1. Introduction

Picornaviruses comprise one of the largest animal virus families (Rueckert, 1990), which includes human rhinovirus, poliovirus, Coxsackie virus, foot-and-mouth disease virus and hepatitis A virus. These small viruses are about 30% RNA by weight and have a mass of $\sim 8{\cdot}5 \times 10^6$ daltons. The icosahedral shell is ~300 Å in diameter and is composed of 60 copies each of four viral coat proteins; VP1, VP2, VP3 and VP4. The structure of human rhinovirus 14 (HRV14) was solved to atomic resolution (Rossmann *et al.*, 1985). The structures of VP1, VP2 and VP3 all have a very similar, eight-stranded, anti-parallel, β-barrel motif. These viral proteins mainly differ in the insertions between the β-strands that form antigenic loops on the virus surface.

Neutralizing immunogenic sites on the surface of HRV14 were defined by locating spontaneous mutations in the viral coat that permitted the virus to escape antibody-mediated neutralization (Sherry & Rueckert, 1985; Sherry *et al.*, 1986). These mutations were clustered into four groups called neutralizing immunogenic (NIm) sites; NIm-IA, NIm-IB, NIm-II and NIm-III (Rossmann *et al.*, 1985).

Monoclonal antibody 17-IA (mAB17-IA) binds to the NIm-IA site, which was defined by natural escape mutations at residues D1091 and E1095 of VP1 on the loop between the β-B and β-C strands of the VP1 β-barrel (the letter designates the amino acid, the first digit identifies the viral protein, and the remaining 3 digits specify the sequence number). Of 24 independent escape mutants at this site, 23 involved changes in charge (Sherry *et al.*, 1986). The exception was a mutation of D1091 to glutamate. The high frequency of charge changes in the escape mutants suggested that electrostatic interactions played an important role in the binding of antibodies to this site.

Here we report the purification, crystallization and structure determination of Fab17-IA. We then demonstrate the accuracy of fitting the Fab atomic model into the cryo-electron microscopy density map and describe the resulting interactions between the virus and antibody.

† Author to whom all correspondence should be addressed.

0022-2836/94/270127-11 $08.00/0

2. Experimental Methods

(a) *Purification of mAb17-IA*

Two different purification schemes were employed to purify mAB17-IA; ion-exchange chromatography using a Mono-Q® column on the FPLC® system and affinity chromatography using protein G.

(i) *Ion-exchange chromatography*

Mouse antibodies were first precipitated from ascites fluid with 60% saturated ammonium sulfate (final concentration). The precipitate, collected after centrifugation for 10 min at 10,000 *g*, was resuspended and dialyzed against 10 mM Tris buffer (pH 7·6), and passed through a 0.45 μm filter before chromatography with a Pharmacia FPLC® (Pharmacia Corp., Pascataway, NJ) system. A 0·5 ml portion of this solution was loaded onto a 1 ml Pharmacia Mono-Q® column and eluted with a linear salt gradient of 0·1 M NaCl/7·0 ml eluant that contained 10 mM Tris (pH 7·6). The flow-rate was 1 ml/min, and the pressure was one MPa. The protein peaks were collected with a Pharmacia FRAC-100® and tested for antibody content with ELISA assays. Goat, anti-mouse Fab_2, antibodies linked to horseradish peroxidase and protein-A linked to alkaline phosphatase were used for detection.

mAb17-IA eluted at ~0·13 M NaCl with approximately 22% of the total amount of mouse antibody eluting at slightly lower salt concentrations. Isotyping experiments were performed on these early peaks using the Screentype® (Boehringer-Mannheim Biochemicals, Indianapolis, IN) ELISA kit and showed that these antibodies were not the same isotype as mAb17-IA and were therefore probably contaminating, endogenous antibodies from the mouse ascites fluid.

The antibody peaks were pooled and precipitated in 70% saturated ammonium sulfate (final concentration). The precipitate, collected after centrifugation for 10 min at 10,000 *g*, was resuspended and dialyzed against 0·1 M sodium phosphate buffer (pH 7·0). The sample was then applied to an S-300® Pharmacia Sepharose column to remove small molecular mass contaminants.

(ii) *Protein G affinity chromatography*

Protein G is a cell-wall protein from β-hemolytic streptococci of the C or G strains and binds to all isotypes of mouse antibodies. To a 3-ml column of protein G matrix (Pharmacia Corp., Pascataway, NJ) equilibrated with 50 mM sodium phosphate (pH 7·0), ~0·5 ml of ascites fluid was applied. The sample was allowed to slowly flow into the column matrix, and washed using the above sodium phosphate buffer. The bound material was eluted with 50 mM sodium citrate buffer (pH 2·0). The eluted material was immediately neutralized with the addition of 1 M sodium phosphate buffer (pH 8·0). The elution of protein was detected using a Pharmacia UV monitor (at 280 nm) and the peaks were collected in 1 ml fractions with a Pharmacia FRAC-100.

(b) *Papain digestion of mAb17-IA*

The solutions of antibody were concentrated by ammonium sulfate precipitation or centrifugation using Centricon 30 (Amicon Corporation, Beverly, MA) to about 2·2 mg/ml (saturation) and dialyzed against 0·1 M sodium phosphate buffer (pH 7·0). The antibody was digested for 17 h at 37 °C in the presence of 25 mM β-mercaptoethanol and at a papain to antibody ratio of 1 : 100 (w/w).

(c) *Purification of Fab17-IA*

After papain digestion, the sample was dialyzed against 10 mM Tris (pH 7·6) and applied to the Mono-Q® column (equilibrated with the same buffer) using a 2-ml sample loop. At this pH, the predominant Fab species with a pI of ~8·3 (isoelectric point focusing results, not shown), did not bind to the column, and eluted in the void volume. The Fab peak was then dialyzed against 10 mM Tris, and concentrated to 5 mg/ml. Purity was tested with reducing and non-reducing SDS-PAGE, ELISA assays, and isoelectric gel electrophoresis. Isoelectropoint analysis of the Fab fragments was performed using a chromatofocusing column (Mono-P). Before each chromatography run, 1 ml of a 1 M NaOH solution was injected onto the column and then equilibrated with 20 mM diethanolamine (pH 9·5). The Fab samples, dialyzed against the latter buffer, were loaded onto the column. The protein was eluted from the Mono P® column with a 1 to 10 dilution of Pharmacia Polybuffer 96® at pH 6·0 (acidified with HCl) at a flow-rate of 0·5 ml/min.

(d) *Crystallization*

Fab17-IA was crystallized at room temperature by the hanging drop method with polyethylene glycol (PEG) 8000 or ammonium sulfate as precipitant. When PEG 8000 was used, the reservoir contained 12% PEG, 3 mM sodium azide and 0·1 M sodium phosphate (pH 6·5 to 7·0). With ammonium sulfate, the reservoir contained 0·1 M sodium phosphate (pH 6·4 to 7·0), 1 mM sodium azide, and ammonium sulfate at 40% saturation. In both cases, the Fab was in 10 mM Tris buffer (pH 7·2), and adjusted to a concentration of 4 mg/ml. The hanging drops contained 10 μl of the Fab solution and 5 μl of the reservoir solution.

(e) *Data collection*

X-ray data were collected from crystal form I at the Cornell High Energy Synchrotron Source (CHESS) using oscillation photography. The oscillation angle was 5° with a 1 to 2 min exposure time/photograph. The wavelength of the X-ray radiation was 1·54 Å and the crystal-to-film distance was 80 mm. The orientations of optically aligned crystals were visually estimated by comparing predicted and recorded reflection patterns. This approximate orientation served as a starting point for systematic optimization of the orientation angle using established methods (Rossmann, 1985). Integrated intensities from the various films were scaled and post-refined in order to accurately determine the cell parameters and mosaicity.

Data were collected on crystal forms II and III using a Siemens area detector attached to a rotating anode X-ray generator. Data were reduced and scaled using the Xengen software package (Howard, 1990).

(f) *Heavy-atom derivatives*

Of the 30 different heavy-atom compounds used on crystal forms I and III, uranyl nitrate hexahydrate ($UO_2(NO_3)_2 \cdot 6H_2O$) was the only usable derivative found for crystal form III. For derivatization, crystals were incubated in a 4 mM uranyl nitrate solution for 40 h.

(g) *Molecular replacement*

The Fab structures of McPC603 (Padlan *et al.*, 1985), HyHEL-5 (Sheriff *et al.*, 1987), and HyHEL-10 (Padlan *et al.*, 1989) were used as molecular replacement models for

phasing data from crystal forms I and III. The models were divided into variable ($V_L \cdot V_H$) and constant ($C_L \cdot C_{H1}$) modules for the cross-rotation function searches. The MERLOT (Fitzgerald, 1988) and locked rotation function (GLRF: Rossmann *et al.*, 1992) programs were used for the calculations on a DEC 3100 workstation (Digital Equipment Corporation, Indianapolis, IN). The variable and constant domains of test Fab molecules were placed in 100 Å^3 cells for analysis by the GLRF program. The cross-rotation function was calculated from data between 3·8 and 8·0 Å with a radius of integration of 30 Å. When the MERLOT package was applied, the entire HyHEL-10 molecule was used as a test model. This model was placed in a 120 Å^3 box and the cross-rotation function was calculated using data between 3·5 and 8 Å with a radius of integration of 20·7 Å. The algorithm of Crowther & Blow (1967) was used for the translation search. XPLOR (Brünger, 1991) was used for further rigid body refinement of the variable and constant modules.

(h) *mAb17-IA variable region sequencing*

Hybridoma-17 cells were lysed in 1% Triton X-100, 50 mM Tris (pH 7·5), 100 mM NaCl and 1 mM EDTA on ice for 10 min. The nuclei were removed by centrifugation at 8000 *g*, 4 °C, for 10 min. The supernatant was deproteinized by 3 extractions with equal volumes of phenol/chloroform/isoamyl alcohol (25 : 24 : 1 by vol.). The total cytoplasmic RNA was precipitated with 2 volumes of absolute ethanol. The pellet was collected by centrifugation at 12,000 *g*, 4 °C, for 20 min, dried and dissolved in diethylpyrocarbonate-treated water.

The poly(A)$^+$ RNA was enriched with oligo(dT)-cellulose. The size and integrity of mAb17-IA heavy and light chain mRNAs were analyzed by electrophoresis in a 1·4% (w/v) agarose gel containing 6·6% (v/v) formaldehyde, transferring to a nitrocellulose paper and hybridizing to a ^{32}P-labeled oligonucleotide primer (5′-GGGGCCAAGTG-GATAGAC-3′) that was complementary to a sequence at the 5′ portion of the gamma constant region and a ^{32}P-labeled oligonucleotide primer (5′-GGTGGGAAGAT-GGATACAGT-3′) that was complementary to a sequence at the 5′ portion of the kappa constant region. Two unique bands corresponding to 1·7 kb and 1·2 kb, respectively, were visualized on the autoradiogram (data not shown). Accession numbers for the derived sequences for the V-regions of mAb17 are: L24919 for the light chain and L24918 for the heavy chain.

The enriched poly(A)$^+$ RNA was sequenced by second-strand synthesis with reverse transcriptase, dideoxynucleotides and a ^{32}P-labeled primer. Four primers were used to sequence the complete variable regions of the gamma and kappa chains, respectively, starting from the 5′ portion of the constant regions. Primers were synthesized at the Biotechnology Center, University of Wisconsin, Madison, then purified through a Sep-Pak C18 Cartridge (part no. 51910, Waters Associates, Milford, MA). The C_L and C_{H1} regions of mAb17-IA were not sequenced because of the highly conserved nature of these domains. Instead, the corresponding amino acid sequences from the Fab fragment HyHEL-10 were substituted.

(i) *Correlation coefficient calculations*

Using 60-fold icosahedral symmetry, an atomic model of the entire Fab17-IA/HRV14 complex with full icosahedral symmetry was constructed based on the modeling results. Structure factors were then calculated using PROLSQ (Hendrickson & Konnert, 1981). An electron density map was computed from these structure factors by Fourier synthesis to a spatial frequency of 0·04 Å^{-1} with an additional temperature factor of 2500 Å^2 imposed to eliminate Fourier ripples. The 2 maps were empirically scaled using correlation coefficients to maximize the agreement of the contrast levels between them. This scale factor was used for all subsequent correlation coefficient calculations. For each of the various maps derived from the atomic coordinates, the coefficients were computed only for those densities within a radial shell that encompassed the bound Fab fragment. This shell included all densities from 155 to 205 Å for all calculations except when the Fab was radially translated from the virion surface in which case a shell from 155 to 245 Å was used.

3. Results and Discussion

(a) *Fab17-IA crystallization*

Fab17-IA crystallized into three different forms; I, II and III. Fab that was obtained from antibodies purified using ion-exchange chromatography and precipitated with PEG 8000, crystallized exclusively in crystal form I (space group $P2_1$, Table 1). With one Fab molecule per asymmetric unit, this crystal form I has a crystal packing density (V_m; Matthews, 1968) of 2·4 Å^3/Da, a value typical for most protein crystals. However, Fab from antibody purified with protein G affinity chromatography and precipitated with PEG 8000 (other crystallization conditions identical), crystallized predominantly in a second crystal form (space group $P2_1$, Table 1). Although crystal forms I and II both belong to the same space group, the *a* axis in form II is twice as large as that in form I. Crystal form II has two Fab molecules in the asymmetric unit, and hence a V_m nearly identical with that of the first crystal form. Fab molecules from antibodies purified with protein G chromatography crystallized into a third form when 40% ammonium sulfate was used as precipitant (Table 1). The space group of this crystal form was $P2_12_12_1$, and the V_m is 2·7 Å^3/Da with one Fab molecule per asymmetric

Table 1

Crystal parameters of the three Fab17-IA crystal forms

	PEG (old)†	PEG (new)‡	AS§
Space group	$P2_1$	$P2_1$	$P2_12_12_1$
a (Å)	41·6	91·8	37·8
b (Å)	90·5	91·6	97·3
c (Å)	63·8	64·4	129·5
β (°)	95·0	100·8	90·0
No. Fab/unit cell	2	4	4
V_m (Å^3/Da)	2·4	2·4	2·7

† Fab17-IA from immunoglobulin purified with ion-exchange chromatography and crystallized with PEG 8000 as precipitant.

‡ Fab generated from mAb17-IA purified with protein G affinity chromatography and crystallized with PEG 8000 as precipitant.

§ Fab17-IA from protein G affinity-purified immunoglobulin and crystallized with ammonium sulfate as precipitant.

Table 2
Data statistics of the various crystal forms and the uranyl derivative

	PEG (old)	PEG (new)	AS	AS (uranyl)
R_{sym}† (%)	9·05	10·0	5·1	8·7
R_{iso} (%)	—	—	—	17·9
No. observations	49,879	21,790	44,321	21,639
No. independent observations	13,643	12,463	12,367	10,192
No. films	74	—	—	—
No. crystals	13	1	1	1
Data collection method	Film	A.D.‡	A.D.‡	A.D.‡

† Note: $R = \frac{\sum_h \sum_i |\langle I \rangle - I_i|}{\sum_h \sum_i \langle I \rangle} \times 100\%$, where $\langle I \rangle$ is the mean of the i observations I_i for reflection h.

‡ Data were collected with the Siemens Area Detector System.

Table 3
Data distribution for the various Fab17-IA crystal forms

Resolution (Å)	PEG (old) (%)	PEG (new) (%)	AS (%)
∞–30	89	33	67
30–15	100	73	99
15–10	100	80	99
10–7·5	100	84	97
7·5–5·0	100	87	98
5·0–3·5	97	72	98
3·5–3·0	86	25	97
3·0–2·75	70	—	82
2·75–2·5	47	—	2
2·5–2·25	17	—	—

unit. Data were collected on all three crystal forms (Tables 2 and 3).

Chromatofocusing studies provided an explanation for the varying crystallization behavior of the Fab fragments. Fab from IgG purified by the two protocols displayed two major pI species, but in different proportions (Figure 1). Thus, the antibody purification scheme might affect the papain digestion pattern. This would produce fragments of different length, which could affect how the Fab molecules crystallize.

(b) *Fab17-IA crystal structure determination*

The only usable heavy-atom derivative was uranyl nitrate hexahydrate when applied to crystal form III. The difference Patterson map showed a single peak on each of the three Harker sections (Figure 2). All three peaks corresponded to a single

Figure 1. Chromatofocusing of 2 different samples of Fab17-IA. The line labeled A is the elution profile of Fab prepared from antibody purified with anion exchange chromatography, whereas line B represents Fab prepared from antibodies purified with protein G chromatography. The y-axis is absorbance in arbitrary units.

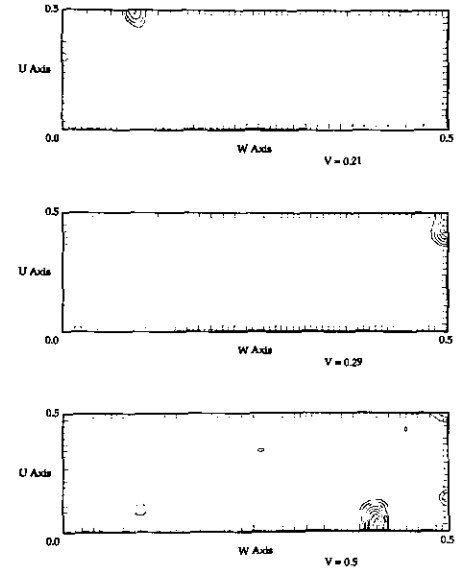

Figure 2. Difference Patterson map of the uranyl nitrate hexahydrate derivative of crystal form III. The 3 Harker sections are shown. The map was scaled to a maximum value of 1000, and the contours start at 40 with increments of 10.

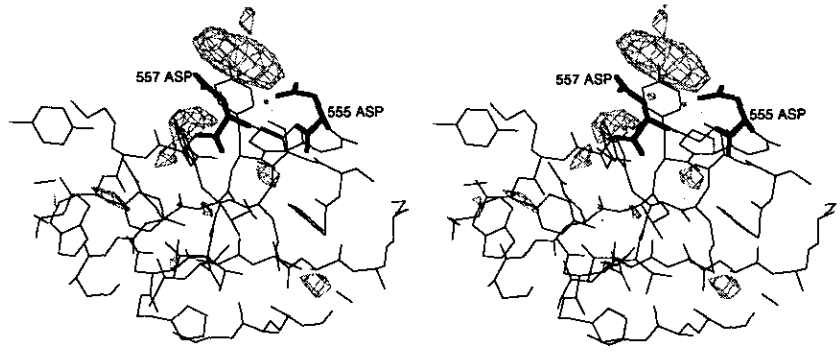

Figure 3. Difference map ($F_H - F_N$) of the uranyl nitrate hexahydrate derivative derived from molecular replacement phases. The atomic model shown is the refined Fab17-IA model (the light chain begins at residue 1 and the heavy chain starts at 501). This heavy-atom position agreed with the difference Patterson map. The uranyl atom is observed to be bound to D557 and D555.

heavy-atom position at $x = 0{\cdot}02$, $y = 0{\cdot}15$ and $z = 0{\cdot}05$. Each peak was at least twice the highest background value and 7 to 12% of the height of the origin peak. This uranyl derivative was refined using the heavy-atom least-squares program (HALSQ; Adams *et al.*, 1969). A Fourier synthesis, using these single isomorphous replacement phases, was calculated, but the electron density was of insufficient quality to trace the protein chain. The electron density was also not sufficiently improved by use of solvent-flattening techniques (Wang, 1985).

Concomitant with the heavy-atom searches, molecular replacement was attempted with the various crystal forms. Of the models tested, HyHEL-10 yielded the best results in the cross-rotation function searches on crystal form III. The peak height/σ for the entire variable and constant modules were both 4·3 with the next highest peaks being 3·1 and 3·8, respectively. Using this model, the translation function was calculated using the Crowther & Blow (1967) formulation. There were well-defined peaks for the intermolecular translation vectors at each of the three Harker sections. In each case, the second highest peak was less than 70% the value of the highest peak. These three peaks were self-consistent and defined the molecular position to be at $x = 0{\cdot}390$, $y = 0{\cdot}415$ and $z = 0{\cdot}275$.

The molecular replacement model was then subjected to rigid body refinement using XPLOR (Brünger, 1991). During this refinement, each of the β-barrels (V_L, V_H, C_L, C_{H1}) was treated as an independent rigid body. After approximately 25 cycles of refinement, the R-factor dropped from 53·4% to 45·1%. To test whether the molecular replacement solution agreed with the heavy atom phases, a difference map ($F_H - F_N$) was calculated using molecular replacement phases. The resulting electron density map showed a single, very large peak (Figure 3) at the same position determined by the heavy-atom difference Patterson. At this time, the residues of the search model variable domains were manually altered to reflect the sequence of Fab17-IA.

The model was then subjected to nine cycles of XPLOR refinement (Brünger, 1991). Each cycle of XPLOR refinement was followed by several cycles of PROLSQ (Hendrickson & Konnert, 1981) refinement. Presently, 69 water molecules are included in the model. With all reflections between 8·0 and 2·7 Å included, and with all atomic thermal factors refined independently, the current R-factor is ~19%, the root-mean-square difference (RMS Δ) of the bond angles is 2·6°, and the RMS Δ of the bond distances is 0·013 Å. The elbow angle of the model is ~161°. The current model fits the density very well (Figure 4).

The accuracy of the current model was further tested by using it to solve the structure of crystal form I. The variable domain, constant domain, and the entire Fab17-IA model each yielded extremely large correlation peaks using either the GLRF or MERLOT programs. The peak height/σ of the variable module, constant module, and entire Fab molecule were 9·3, 5·5 and 7·1 with the next highest peaks being 3·6, 3·7 and 3·7, respectively.

With this rotation function solution, the Fab17-IA structure was then used as a search model in the translation function search of crystal form I. Using data between 6 and 3 Å, the height/σ of the highest translation function peak was 11·0, which was more than three times that of the next highest peak. This molecular replacement solution was then refined with a single cycle of XPLOR refinement. The crystallographic R-factor for all data between 8·0 and 2·7 Å resolution is ~19%. This gave final proof that the current model accurately describes the structure of Fab17-IA in two different crystal forms. Refinement of both crystal forms is in progress.

(d) *Accuracy of atomic modeling of Fab17-IA/HRV14 complex*

The structure of the Fab17-IA/HRV14 complex was determined to ~25 Å resolution using cryo-electron microscopy and image reconstruction techniques (Smith *et al.*, 1993*a*). For these studies, it was assumed that the elbow angle of the bound Fab was equivalent to that observed in the crystal structure

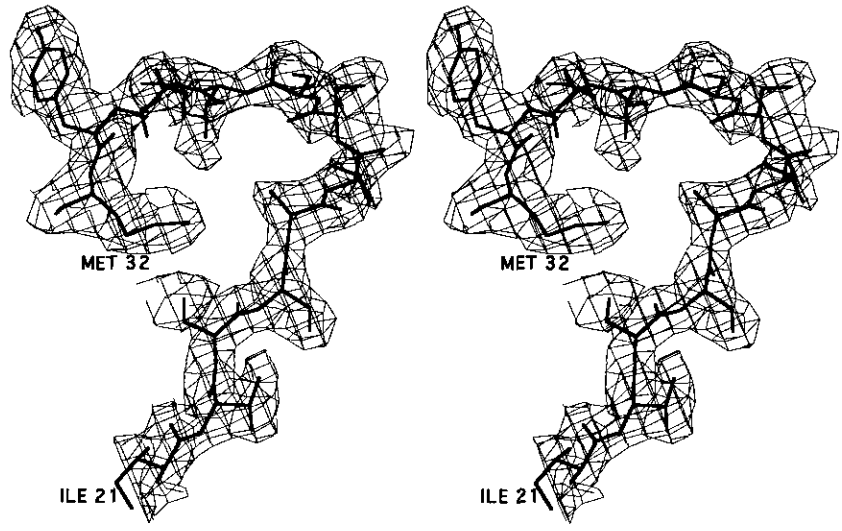

Figure 4. Omit map of the CDR1 loop of the light chain. For this electron density map, this hypervariable loop was omitted from the structure, and the resulting phases were used in the Fourier calculations ($2F_o - F_c$). The quality of this section of electron density is typical of most of the Fourier map.

(161°). The atomic model of Fab17-IA was manually fitted to the molecular envelope. To evaluate the accuracy of Fab positioning, the Fab model was displaced from its optimal position by a series of translations and rotations. The resulting Fab/HRV14 model was then used to calculate a set of structure factors from which an electron density map could be produced for comparison with the image reconstruction. First, the Fab model was systematically moved over the HRV14 surface (approximated by an X-Y plane). The highest correlation coefficient occurred at the original position fitted by eye and dropped off significantly for translations of the Fab molecule at less than 5 Å (Figure 5(a)). A less striking, but significant drop in the correlation coefficient occurred when the Fab molecule was translated away from the HRV14 surface along the long axis of the Fab molecule

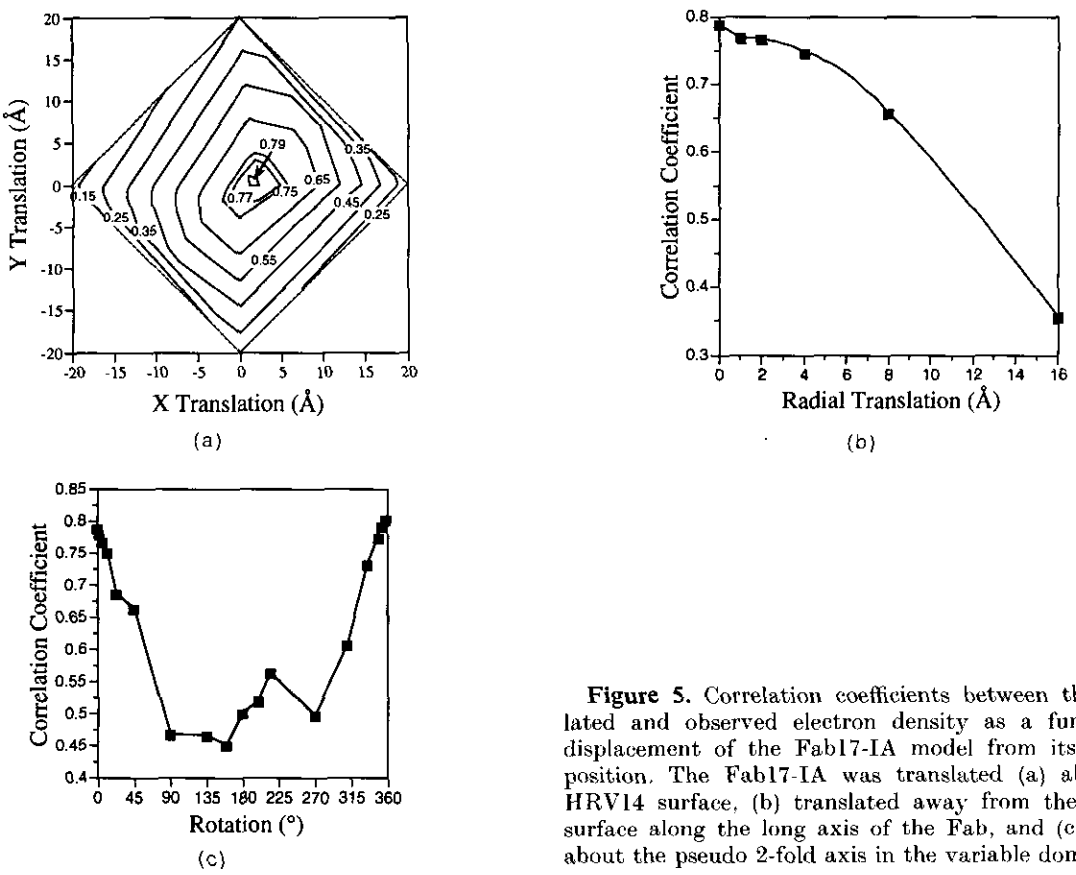

Figure 5. Correlation coefficients between the calculated and observed electron density as a function of displacement of the Fab17-IA model from its optimal position. The Fab17-IA was translated (a) about the HRV14 surface, (b) translated away from the HRV14 surface along the long axis of the Fab, and (c) rotated about the pseudo 2-fold axis in the variable domain.

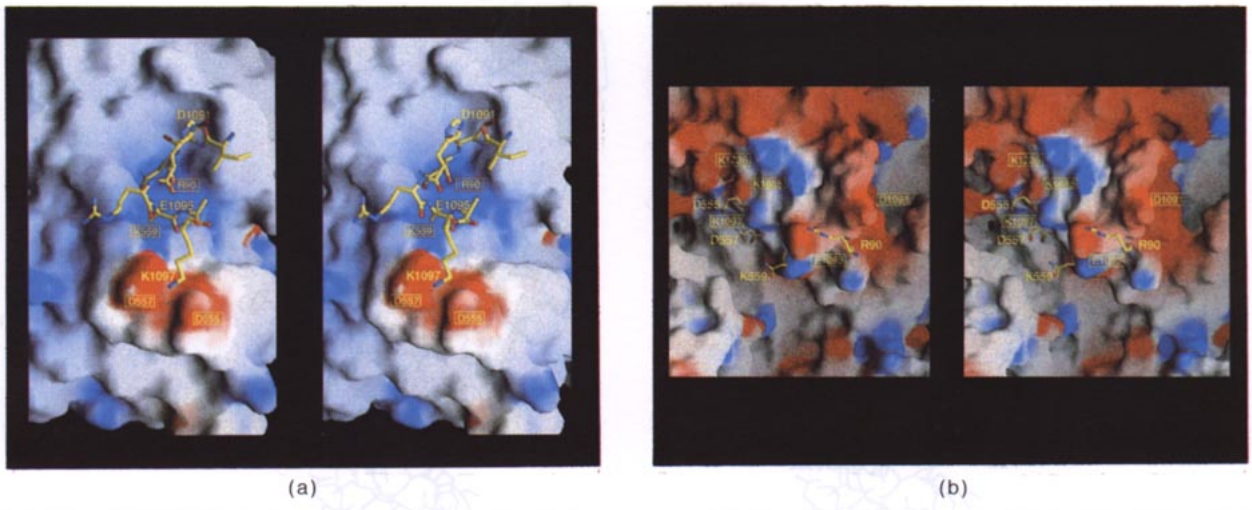

Figure 6. Complementary surfaces of the Fab and virus with the electrostatic potential mapped onto the molecular surfaces. Negative and positive potentials are represented by red and blue colors, respectively. Above each surface are stick figures of residues that form proposed, key contacts with the illustrated surface. The charged residues on the molecular surface renderings are identified by boxed labels, whereas the charged "stick" residues are labeled without boxes. (a) Space-filling rendering of the Fab17-IA hypervariable region with the residues of HRV14 comprising the VP1 B-C loop (residues 1090 to 1097: IDNHREAK) shown as a stick figure. The other lysine residues involved in antibody binding (see (b) are not shown. The view is from the viral surface looking towards the antibody hypervariable region. (b) A portion of the HRV14 surface with selected, charged residues from Fab17-IA included as stick figures. The view here is from the antibody variable region looking towards the viral surface. The nearest 5-fold axis lie to the North of the diagram.

(Figure 5(b)). Also, the correlation coefficient dropped sharply upon rotation of the model about the pseudo 2-fold axis in the $V_H \cdot V_L$ module (Figure 5(c)); deviations from the original rotational orientation as small as 3 to 6° were easily detected. Another Fab with an elbow angle of ~180° (Kol; Marquart *et al.*, 1980), gave a poorer fit to the density with a correlation coefficient of 0·70 in contrast to a correlation coefficient of 0·87 with Fab17-IA. In addition, Kol contacted the viral surface mostly with a single CDR loop. This supports the assumption that the elbow angle observed in the crystal structure of Fab17-IA is a good approximation of that observed in the bound Fab structure.

(c) *Interactions between HRV14 and Fab17-IA*

The final result, obtained by modeling the atomic structures of the Fab and virus into the cryo-electron microscopy image reconstruction, showed extensive charge and shape complementary at the binding interface (Figure 6). The left stereoimage (Figure 6(a)) depicts the surface of the antigen binding site on the antibody and the right stereoimage (Figure 6(b)) shows the corresponding surface of the NIm-IA site on the virus.

The stick model in Figure 6(a) represents the protruding portion of the VP1 B-C loop that contains the NIm-IA site of the virus. As shown here, the two acidic residues comprising the NIm-IA site (D1091 and E1095) insert into the deep recesses of a positively charged pocket lying between the hypervariable regions of the heavy and light chains in the antibody. Most of the charge in this pocket comes from R90 and K559 (Fab17-IA residues are numbered sequentially with the light and heavy chains starting with 1 and 501, respectively). Because most escape mutations (23 of 24) at these two residues represented charge alterations, it was previously suggested that electrostatic charge at this loop might be crucial for antibody recognition (Sherry & Rueckert, 1985). The structural basis for such charge recognition is clearly evident in Figure 6(a). It should be noted that some of the contact distances between these side-chains and the hypervariable region are shorter than what would be acceptable van der Waals contact distances. This may be due to small errors in the positioning of the atomic Fab model or it might reflect relatively small conformational changes that could occur as the virus and antibody accommodate each other during binding.

Even greater confidence in this complex structure emerged when the antibody interactions were examined from the opposite perspective (Figure 6(b)). Here, the VP1 B-C loop shown in Figure 6(a) appears as a prominent tower capped with the negatively charged (red) residues D1091 and E1095, while the complementary charged residues from the antibody are depicted as stick models. The deep depression lying to the South of this tower corresponds to the canyon that binds the cellular ICAM-1 receptor molecule (Olson *et al.*, 1993). The canyon continues to the East and West as it encircles a 5-fold axis that is to the North). More importantly for our purposes, the saddle to the Northwest of this tower contains a cluster of three lysine residues

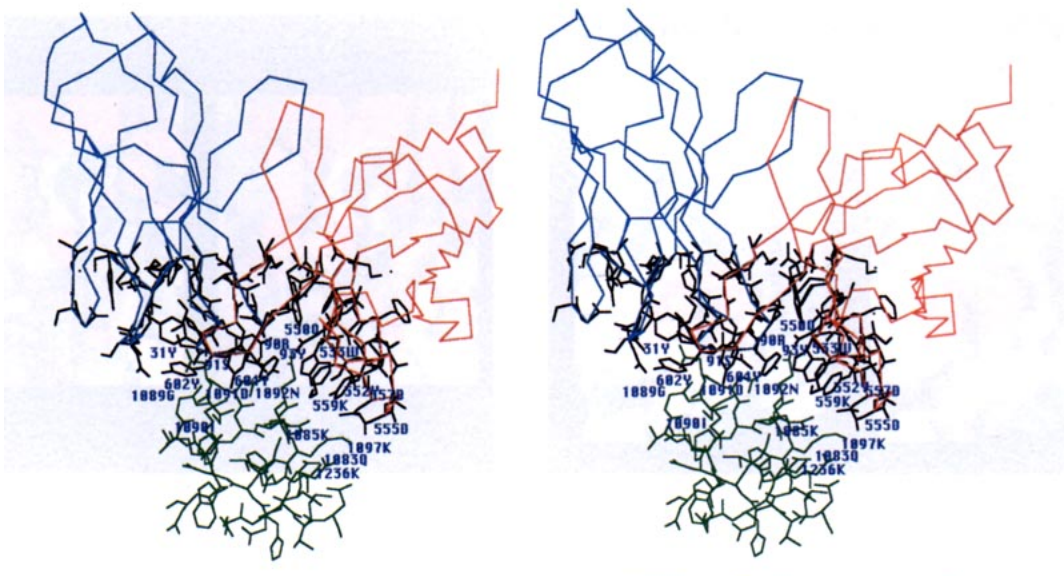

Figure 7. Interface between the bound Fab17-IA and the surface of HRV14. The C^{α} atoms of the light chain are blue, those of the heavy chain are red, the residues of HRV14 around the contact region are green, and the residues of Fab17-IA about the contact site are black.

(K1097, K1085 and K1236) corresponding to the base of the VP1 B-C loop. These three lysine residues interact with an acidic protuberance (D555 and D557) that lies on the rim of the Fab alkaline binding pocket (Figure 6(a)). This interaction suggested that these three lysine residues might be involved in antibody recognition even though no change at these sites had been observed in the original sample of 24 different escape mutants (Sherry & Rueckert, 1985).

To test this hypothesis, all three lysine residues were mutated and the resulting effects on antibody binding were measured. In three independent experiments, mutating residues K1097, K1085 and K1236 to glutamate decreased the binding affinities 36·0, 3·9 and 2·4-fold, respectively. The relatively small effects of mutations at K1085 and K1236 are likely due to their peripheral location near the edge of the virus-antibody interface. K1085 and K1236 may play a small role in antibody binding perhaps by contributing to the electrostatic field in that particular area of HRV14. These results agree exceedingly well with the modeled complex structure. D555 and D557 are observed to bind directly over K1097 (see also Figure 6(a)) and are adjacent to K1085 and K1236. Furthermore, the distance between these lysine residues and the two aspartate residues is proportional to their role in antibody binding. Mutations at these lysine residues were probably not observed amongst natural escape mutants because selection was limited to those mutants with viability equivalent to the native virus.

The remaining residues in the Fab hypervariable region envelope the entire NIm-IA loop with both polar and non-polar interactions (Figure 7). Shown here are V_L and V_H domains (top) bound to the VP1 B-C loop region (bottom). The CDR3 loop of the heavy chain (e.g. Y682 and Y684 to the left of the VP1 B-C loop) seems to form a hydrophobic flap over the North side of the NIm-IA loop (the side closest to the neighboring 5-fold axis). Y602 and Y604 of Fab17-IA may contact I1090 and G1089 of HRV14. In addition, Y31 may also contact this region of HRV14 by binding near D1091. The structure of this interface is clearly only a first approximation of the actual structure. For example, if the side-chain of D1091 were to rotate to another sterically acceptable position, it would be positioned to form better coulombic interactions with several basic residues of Fab17-IA. An initial energy minimization calculation was performed on the complex using XPLOR (data not shown). The close contacts were easily accommodated by relatively small distortions in the hypervariable contact region. Most notably, the main chain of the heavy chain CDR3 loop moved slightly away from the NIm-IA loop. This motion agrees with the observed high thermal factors for those residues in the Fab17-IA atomic model. The residues of Fab17-IA that are shown here to be in close contact with HRV14 are quite homologous to those used by other Fabs to bind antigen (Table 4). The one notable exception is that the light chain CDR2 loop is not observed to contact the virion surface. However, the absence of contact between this loop and the bound antigen is not uncommon (Table 4).

The framework region of Fab17-IA also appeared to contact the HRV14 surface on the side (South) of the canyon opposite to the antibody binding site (Smith *et al.*, 1993*a*,*b*). At least three of the β strand/β strand turns of the C_{H1} domain may be involved (Figure 8). Unlike the hypervariable contacts, most of these possible interactions seem to be of a polar nature. This contact is unlikely to contribute to the specificity of antigen recognition. Recall that

Table 4
Alignment of Fab CDR regions

	Light chain								Heavy chain						
	1	2	3	4	5	6	7		1	2	3	4	5	6	7
											T	**T**			
24	S	S	R	R	K	T	R	31	D	S	**S**	**G**	D	N	D
25	A	A	A	A	A	G	S	32	Y	F	**D**	**Y**	F	D	Y
26	S	T	S	S	S	S	S	33	**W**	**W**	**Y**	G	**Y**	Y	**W**
27	S	**S**	Q	G	Q	S	Q	34	I	V	W	V	M	Y	M
27A					S	S	S	35	**E**	N	S	N	E	T	N
27B					L	N	L								
27C					L	I	V		**W**					**W**	
27D					N	**H**		50	**E**	**Q**	**Y**	M	A	Y	Q
27E					S		S	51	I	I	V	I	S	V	I
27F					G			52	L	**Y**	**S**	**W**	**R**	F	R
28			S	N	N	G	N	52A	P				N		N
29	S	S	I	I	Q	A	G	52B					K		K
30	V	V	**G**	**H**	K	**G**	N	52C					G		P
31	**N**	N	**N**	N	N	**N**	T	53	G	G	**Y**	**G**	N	**Y**	Y
32	**Y**	**Y**	**N**	**Y**	F	H	**Y**	54	**S**	**D**	**S**	**D**	K	H	N
33	M	M	L	L	L	V	L	55	G	G	G	G	Y	G	Y
34	Y	H	H	A	A	K	**R**	56	**S**	**D**	**S**	N	R	**T**	E
								57	**T**	N	T	T	R	S	T
				Y				58	**N**	**K**	**Y**	D	E	D	Y
50	**D**	S	**Y**	**Y**	G	H	K	59	Y	Y	Y	Y	Y	D	Y
51	T	S	A	T	A	N	V	60	H	N	N	N	S	T	S
52	S	S	S	T	S	N	S	61	E	G	P	S	A	T	D
53	K	N	**Q**	T	T	A	N	62	R	K	S	A	S	P	S
54	L	L	S	L	R	R	R	63	F	F	L	L	V	L	V
55	A	A	I	A	E		F	64	K	K	K	K	K	R	K
56	S	S	S	D	S		S	65	G	G	S	S	G	S	G
89	Q	Q	Q	Q	Q	N	S	95	**G**	S	**W**	E	**N**	N	S
90	Q	Q	Q	H	N	S	Q	96	N	G	D	**R**	Y	**L**	Y
91	**W**	**R**	**S**	**F**	**D**	**Y**	**S**	97	**Y**	N	G	**D**	Y	**I**	Y
92	**G**	**S**	**N**	**W**	H	D	T	98	D	**Y**		**Y**	G	**A**	G
93	**R**	**S**	S	**S**	S	R	H	99		P		**R**	S	G	M
94	N	**Y**	W	T	**Y**	**S**	V	100				L	T	C	
95	**P**	P	P	P	**P**	**L**	P	100A						I	
96		I	**Y**	R	**L**	R	**W**	100I		**Y**			**W**		
97	T	T	T	T	T	V	T	100J		A			Y		
								100K	F	M			F		
								101	D	D	D	D	D	D	D
								102	G	Y	Y	Y	V	V	Y

The columns represent the hypervariable (CDR) regions of the following Fabs: (1) HyHEL-5 (Sheriff *et al.*, 1987), (2) Fab17-IA, (3) HyHEL-10 (Padlan *et al.*, 1989), (4) D1.3 (Amit *et al.*, 1986), (5) McPC603 (Padlan *et al.*, 1985), (6) NEWM (Amzel *et al.*, 1974) and (7) 4-4-20 (Herron *et al.*, 1989). HyHEL-5, HyHEL-10 and D1.3 were all raised against lysozyme. This Table was compiled by Kabat *et al.* (1987). For comparison, some Fabs that bind small antigens are also listed: McPC603, NEWM and 4-4-20, which bind phosphatidyl choline, a variety of haptens and fluoresyl hapten, respectively. The residues in contact with bound antigen are identified in bold face and underlined. For this Table, the sequence of Fab17-IA was aligned according to previously published nomenclature (Kabat *et al.*, 1987).

mAB17-IA was shown to bind bivalently across icosahedral 2-fold axes (Mosser *et al.*, 1989; Leippe, 1991; Smith *et al.*, 1993*a*,*b*). Such an unusual contact between the framework region of the antibody and the HRV14 surface may be necessary to allow the antibody to bridge across two NIm-IA sites. Mutational studies on HRV14 are underway to determine the importance of these residues in antibody binding.

From these results, this antibody clearly recognizes not just the VP1 B-C loop but, in fact, the entire three-dimensional structure of this region. This is supported by results that show a lack of response of mAb17-IA to HRV14 in Western assays (C. Porta, personal communication) and the lack of binding of the NIm-IA peptide (residues 1090 to 1097: IDNHREAK) to Fab17-IA (unpublished results).

(f) *Antibody-mediated neutralization of HRV14*

Biochemical studies of mAb17-IA showed that the binding of this antibody to HRV14 causes a shift in the isoelectric point of the virus from approximately 7·0 to less than 4·0 (Colonno *et al.*, 1989). However, electron microscopy studies showed that neither this Fab nor the intact antibody appear to cause gross conformational changes in the virion capsid (Smith *et al.*, 1993*a*,*b*). These results suggest that either the pI shift is not correlated to a large conformational change in the virus or that the pI shift requires, in addition to antibody binding, the presence of non-physiological conditions such as those needed for isoelectric focusing (e.g. low ionic strength and unusual buffers). Alternatively, the pI changes may be due to alterations in surface accessibility and not due to any structural changes. The observation of short atomic contact distances at the Fab/virus interface suggest that small conformational changes, of the magnitude recently observed in high-resolution crystallographic studies (Rini *et al.*, 1992), may occur in the Fab or virus, or both, upon antibody binding.

Our results suggest that the mechanism of neutralization for mAb17-IA probably does not involve gross conformational changes in the virions. What then is the most probable mechanism? mAb17-IA is known to both neutralize and block attachment of HRV14 to host cells at a stoichiometry of about five to ten antibodies per virion (Leippe, 1991; Lee, 1992). This result is consistent with the fact that bound mAb17-IA (and Fab17-IA) occlude the receptor binding site (Smith *et al.*, 1993*a*,*b*; Olson *et al.*, 1993). Also, mAb17-IA stabilizes the virus against acid-induced denaturation (Lee, 1992). This suggests that a secondary mechanism of neutralization might be the inhibition of viral uncoating. However, no compensatory escape mutation that is distal to the antigenic sites has been identified. Such mutations are possible since, in the case of WIN compounds, distal mutations that compensate for drug-mediated stabilization have been observed (Heinz *et al.*, 1989). Neither of these proposed mechanisms requires the induction of large conformational changes in the virion.

The Fab17-IA/HRV14 complex has been crystallized (Smith & Chase, 1992), but the crystals presently diffract only to ~4 to 5 Å resolution (unpublished results). Knowledge of the structure of

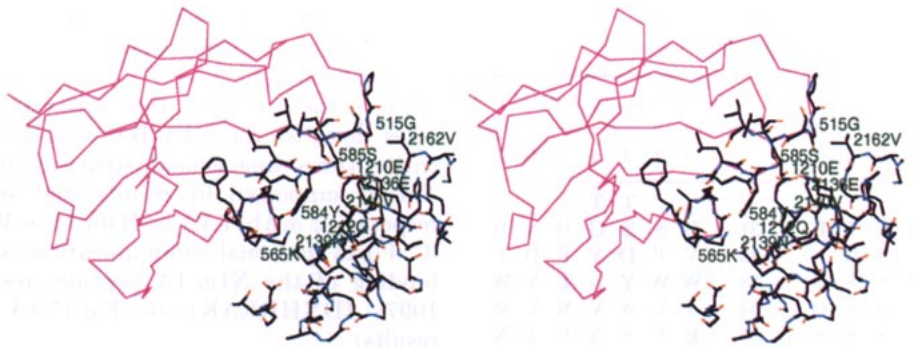

Figure 8. Portion of the framework region of Fab17-IA that may be in contact with the HRV14 surface. The position of the Fab17-IA molecule is as previously determined by electron microscopy (Smith *et al.*, 1993*a*,*b*). The RNA interior is towards the bottom of the diagram, an icosahedral 5-fold axis is towards the left-hand side, and the South wall of the canyon is on the right-hand side. The C^{α} backbone of the C_H domain is portrayed in green and the C, N and O atoms are depicted in black, blue and red, respectively. Residues that might be in contact with each other are labeled.

the complex, even at moderate resolution, should improve the mapping of the hypervariable contact regions, help ascertain the importance of the framework contacts with the South wall of the HRV14 canyon, and determine the existence and magnitude of smaller-scale conformational changes. In addition, studies are underway to examine other antibodies to this and other NIm sites to test for possible correlations between the mode of antibody binding and neutralization efficacy.

We thank Dr Michael Rossmann for enthusiastic support and initial advice. This work was supported by grants from the National Institutes of Health (GM10704 to T.J.S., AI31960 to R.R.R. and GM33050 to T.S.B.), from the National Science Foundation (MCB 9206305 to T.S.B.) and the Lucille P. Markey Charitable Trust (Purdue Structural Biology Center). FRODO (Jones, 1982) and MacInPlot II (Smith, 1993) were used for diagrams 3, 4, 7 and 8. Figure 6 was made using GRASP program (Nicholls, 1993). This structure will be deposited into the Brookhaven Protein Data Bank.

References

Adams, M. J., Haas, D. J., Jeffery, B. A., McPherson, A., Jr, Mermall, H. L., Rossmann, M. G., Schevitz, R. W. & Wonacott, A. J. (1969). Low resolution study of crystalline L-lactate dehydrogenase. *J. Mol. Biol.* **41**, 159–188.

Amit, A. G., Mariuzza, R. A., Phillips, S. E. V. & Poljak, R. J. (1986). Three-dimensional structure of an antigen-antibody complex at 2·8 Å resolution. *Science*, **233**, 747–753.

Amzel, L. M., Phillips, R. J., Saul, F., Varga, J. M. & Richards, F. F. (1974). The three dimensional structure of a combining region-ligand complex of immunoglobulin NEW at 3·5 Å resolution. *Proc. Nat. Acad. Sci., U.S.A.* **71**, 1427–1430.

Brünger, A. T. (1991). Simulated annealing in crystallography. *Annu. Rev. Phys. Chem.* **42**, 197–233.

Colonno, R. J., Callahan, P. L., Leippe, D. M. & Rueckert, R. R. (1989). Inhibition of rhinovirus attachment by neutralizing monoclonal antibodies and their Fab fragments. *J. Virol.* **63**, 36–42.

Crowther, R. A. & Blow, D. W. (1967). A method of positioning a known molecule in an unknown crystal structure. *Acta Crystallogr.* **23**, 544–548.

Fitzgerald, P. M. D. (1988). MERLOT, an integrated package of computer programs for the determination of crystal structures by molecular replacement. *J. Appl. Crystallogr.* **21**, 273–278.

Heinz, B. A., Rueckert, R. R., Shepard, D. A., Dutko, F. J., McKinlay, M. A., Francher, M., Rossmann, M. G., Badger, J. & Smith, T. J. (1989). Genetic and molecular analysis of spontaneous mutants of human rhinovirus 14 resistant to an antiviral compound. *J. Virol.* **63**, 2476–2485.

Hendrickson, W. A. & Konnert, J. H. (1981). *Stereochemically Restrained Crystallographic Least-squares Refinement of Macromolecule Structures.* Pergamon Press, Oxford.

Herron, J. N., He, S.-M., Mason, M. L., Voss, E. W., Jr & Edmunson, A. B. (1989). Three-dimensional structure of a fluorescein-Fab complex crystallized in 2-methyl-2,4-pentandiol. *Proteins: Struct. Funct. Genet.* **5**, 271–280.

Howard, A. J. (1990). *A Guide to Macromolecular X-ray Data Reduction for the Siemens Area Detector System: the XENGEN System Version 2.0.* Gaithersburg, MD: Protein Engineering Department, Genex Corporation.

Icenogle, J., Shiwen, H., Duke, G., Gilbert, S., Rueckert, R. & Anderegg, J. (1983). Neutralization of poliovirus by a monoclonal antibody: kinetics and stoichiometry. *Virology*, **127**, 412–425.

Jones, T. A. (1982). *A Graphics Model Building and Refinement System for Macromolecules.* Clarendon Press, Oxford.

Kabat, E. A., Wu, T. T., Reid-Miller, M., Perry, H. M. & Gottesman, K. S. (1987). *Sequences of Proteins of Immunological Interests.* No. U.S. Department of Health and Human Services, Public Health Service, National Institutes of Health, Bethesda, MD.

Lee, W. M. (1992). Ph.D. thesis, University of Wisconsin.

Leippe, D. M. (1991). Ph.D. thesis, University of Wisconsin.

Marquart, M., Deisenhofer, J., Huber, R. & Palm, W. (1980). Crystallographic refinement and atomic models of the intact immunoglobulin molecule Kol and its antigen-binding fragment at 3·0 Å and 1·9 Å resolution. *J. Mol. Biol.* **141**, 369–391.

Matthews, B. W. (1968). Solvent content of protein crystals. *J. Mol. Biol.* **33**, 491–497.

Mosser, A. G., Leippe, D. M. & Rueckert, R. R. (1989). *Neutralization of Picornaviruses: Support for the Pentamer Bridging Hypothesis.* American Society for Microbiology, pp. 155–167, Washington, DC.

Nicholls (1993). *GRASP: Graphical Representation and Analysis of Surface Properties.* Columbia University.

Olson, N. H., Kolatkar, P. R., Oliveira, M. A., Cheng, R. H., Greve, J. M., McClelland, A., Baker, T. S. & Rossmann, M. G. (1993). Structure of a human rhinovirus complexed with its receptor molecule. *Proc. Nat. Acad. Sci., U.S.A.* **90**, 507–511.

Padlan, E. A., Cohen, G. H. & Davies, D. R. (1985). *Ann. Inst. Pasteur/Immunol.* **136C**, 271–276.

Padlan, E. A., Silverton, W. W., Sheriff, S., Cohen, G. H., Smith-Gill, S. J. & Davies, D. R. (1989). Structure of an antibody-antigen complex: crystal structure of the HyHEL-10 Fab-lysozyme complex. *Proc. Nat. Acad. Sci., U.S.A.* **86**, 5938–5942.

Rini, J. M., Schulze-Gahmen, U. & Wilson, I. A. (1992). Structural evidence for induced fit as a mechanism for antibody-antigen recognition. *Science*, **255**, 959–965.

Rossmann, M. G. (1985). Determining the intensity of Bragg reflections from oscillation photographs. *Methods Enzymol.* **114**, 237–280.

Rossmann, M. G., Arnold, E., Erickson, J. W., Frankenberger, E. A., Griffith, J. P., Hecht, H. J., Johnson, J. E., Kamer, G., Luo, M., Mosser, A. G., Rueckert, R. R., Sherry, B. & Vriend, G. (1985). Structure of a human common cold virus and functional relationship to other picornaviruses. *Nature (London)*, **317**, 145–153.

Rossmann, M. G., McKenna, R., Tong, L., Xia, D., Wu, H. & Choi, H. (1992). Molecular replacement real-space averaging. *J. Appl. Crystallogr.* **25**, 166–180.

Sheriff, S., Silverton, E. W., Padlan, E. A., Cohen, G. H., Smith-Gill, S. J., Finzel, B. C. & Davies, D. R. (1987). Three-dimensional structure of an antibody-antigen complex. *Proc. Nat. Acad. Sci., U.S.A.* **84**, 8075–8079.

Sherry, B., Mosser, A. G., Colonno, R. J. & Rueckert, R. R. (1986). Use of monoclonal antibodies to identify four neutralization immunogens on a common cold picornavirus, human rhinovirus 14. *J. Virol.* **57**, 246–257.

Sherry, B. & Rueckert, R. R. (1985). Evidence for at least two dominant neutralization antigens on human rhinovirus 14. *J. Virol.* **53**, 137–143.

Smith, T. J. (1993). MacInPlot II—an updated program to display electron density and atomic models on the MacIntosh personal computer. *J. Appl. Crystallogr.* **26**, 496–498.

Smith, T. J. & Chase, E. S. (1992). Purification and crystallization of intact human rhinovirus complexed with a neutralizing Fab. *Virology*, **191**, 600–606.

Smith, T. J., Olson, N. H., Cheng, R. H., Liu, H., Chase, E., Lee, W. M., Leippe, D. M., Mosser, A. G., Ruekert, R. R. & Baker, T. S. (1993*a*). Structure of human rhinovirus complexed with Fab fragments from a neutralizing antibody. *J. Virol.* **67**, 1148–1158.

Smith, T. S., Olson, N. H., Cheng, R. H., Chase, E. S. & Baker, T. S. (1993*b*). Structure of a human rhinovirus-bivalent antibody complex: implications for virus neutralization and antibody flexibility. *Proc. Nat. Acad. Sci., U.S.A.* **90**, 7015–7018.

Wang, B. C. (1985). Resolution of phase ambiguity in macromolecular crystallography. *Methods in Enzymol.* **115**, 90–112.

Edited by I. A. Wilson

(Received 4 August 1993; accepted 5 April 1994)